

Multiscale structural complexity analysis of neuronal activity in suprachiasmatic nucleus: Insights from tetrodotoxin-induced disruptions

Ping Wang(王萍), Changgui Gu(顾长贵), and Huijie Yang(杨会杰)

Citation: Chin. Phys. B, 2025, 34 (**4**): 048701. DOI: 10.1088/1674-1056/adaccd
Journal homepage: http://cpb.iphy.ac.cn; http://iopscience.iop.org/cpb

What follows is a list of articles you may be interested in

Free running period affected by network structures of suprachiasmatic nucleus neurons exposed to constant light

Jian Zhou(周建), Changgui Gu(顾长贵), Yuxuan Song(宋雨轩), and Yan Xu(许艳)
Chin. Phys. B, 2023, 32 (**9**): 098701. DOI: 10.1088/1674-1056/acd7ce

Comparison of sleep timing of people with different chronotypes affected by modern lifestyle

Ying Li(李莹), Ji-Chen Guo(郭纪辰), and Xue Wang(王雪)
Chin. Phys. B, 2023, 32 (**6**): 068702. DOI: 10.1088/1674-1056/acbf1f

Entrainment range affected by the difference in sensitivity to light-information between two groups of SCN neurons

Bao Zhu(朱宝), Jian Zhou(周建), Mengting Jia(贾梦婷), Huijie Yang(杨会杰), Changgui Gu(顾长贵)
Chin. Phys. B, 2020, 29 (**6**): 068702. DOI: 10.1088/1674-1056/ab8897

Entrainment range affected by the heterogeneity in the amplitude relaxation rate of suprachiasmatic nucleus neurons

Chang-Gui Gu(顾长贵), Ping Wang(王萍), Hui-Jie Yang(杨会杰)
Chin. Phys. B, 2019, 28 (**1**): 018701. DOI: 10.1088/1674-1056/28/1/018701

Collective behaviors of suprachiasm nucleus neurons under different light-dark cycles

Gu Chang-Gui (顾长贵), Zhang Xin-Hua (张新华), Liu Zong-Hua (刘宗华)
Chin. Phys. B, 2014, 23 (**7**): 078702. DOI: 10.1088/1674-1056/23/7/078702

Multiscale structural complexity analysis of neuronal activity in suprachiasmatic nucleus: Insights from tetrodotoxin-induced disruptions

Ping Wang(王萍)[1], Changgui Gu(顾长贵)[2,†], and Huijie Yang(杨会杰)[2]

[1] *School of Science, Jiangsu University of Science and Technology, Zhenjiang* 212100, *China*
[2] *Business School, University of Shanghai for Science and Technology, Shanghai* 200433, *China*

(Received 13 November 2024; revised manuscript received 18 December 2024; accepted manuscript online 22 January 2025)

The suprachiasmatic nucleus in the hypothalamus is the master circadian clock in mammals, coordinating physiological processes with the 24-hour day–night cycle. Comprising various cell types, the suprachiasmatic nucleus (SCN) integrates environmental signals to maintain complex and robust circadian rhythms. Understanding the complexity and synchrony within SCN neurons is essential for effective circadian clock function. Synchrony involves coordinated neuronal firing for robust rhythms, while complexity reflects diverse activity patterns and interactions, indicating adaptability. Interestingly, the SCN retains circadian rhythms in vitro, demonstrating intrinsic rhythmicity. This study introduces the multiscale structural complexity method to analyze changes in SCN neuronal activity and complexity at macro and micro levels, based on Bagrov *et al*.'s approach. By examining structural complexity and local complexities across scales, we aim to understand how tetrodotoxin, a neurotoxin that inhibits action potentials, affects SCN neurons. Our method captures critical scales in neuronal interactions that traditional methods may overlook. Validation with the Goodwin model confirms the reliability of our observations. By integrating experimental data with theoretical models, this study provides new insights into the effects of tetrodotoxin (TTX) on neuronal complexities, contributing to the understanding of circadian rhythms.

Keywords: suprachiasmatic nucleus, circadian rhythm, complexity, synchrony, multiscale structural complexity

PACS: 87.18.Yt, 05.45.Xt

DOI: 10.1088/1674-1056/adaccd **CSTR:** 32038.14.CPB.adaccd

1. Introduction

The suprachiasmatic nucleus (SCN), located in the hypothalamus, is recognized as the master circadian clock in mammals, orchestrating various physiological processes to align with the 24-hour day-night cycle.[1–4] Although the SCN is a small structure, it is composed of multiple cell types that contribute to its complex structure and function.[5–7] For example, its roles as both an oscillator and pacemaker are realized through dynamic processes that span various spatial scales, ranging from genetic and neuronal interactions to the SCN network and inter-network interactions.[8] In fact, even electrical activity data from a single neuron can reveal both circadian and second-scale rhythmic components, underscoring the complexity of the system, from individual neurons to the organization of the SCN as a whole. Each cell type within the SCN performs distinct roles, contributing to the overall complexity and robustness of the circadian rhythms it generates. This intricate structure allows the SCN to integrate diverse environmental signals and modulate physiological processes accordingly.

Understanding the complexity and synchrony within SCN neurons is crucial, as these properties are fundamental to the effective functioning of the circadian clock.[9–11] Synchrony refers to the coordinated firing of neurons, which is essential for robust rhythmic output.[12] Complexity, meanwhile, reflects the richness of neuronal activity patterns and interactions, indicating the system's capacity to adapt and respond to various signals. This complexity is a vital characteristic of neuronal activity, showcasing the dynamic behavior and adaptability of the system. Interestingly, even when the SCN is isolated from the brain, it continues to exhibit robust circadian rhythms in vitro for several days, underscoring its intrinsic rhythmicity and the inherent complexity of its neuronal network.[13,14]

Tetrodotoxin (TTX) is a powerful neurotoxin that blocks sodium channels, effectively inhibiting action potentials in neurons and reducing their coupling strength.[13,15] Abel *et al*. applied TTX to slices of mouse explants and obtained bioluminescent reporter data from individual neurons, categorizing these data into three stages: pre-TTX, during-TTX, and post-TTX.[16] These data provide a unique opportunity to study how disruptions in electrical activity affect neuronal synchrony and complexity. For instance, Abel *et al*. applied maximal information coefficient statistics to the data from different stages, inferring that the functional connectivity network in the SCN exhibits small-world characteristics. Additionally, Gu *et*

†Corresponding author. E-mail: gu_changgui@163.com

© 2025 Chinese Physical Society and IOP Publishing Ltd. All rights, including for text and data mining, AI training, and similar technologies, are reserved.

al. measured the synchronization degree and the disassortativity coefficient of the network structure, finding that the SCN network is a disassortative network.[17]

These studies offer valuable insights into the effects of TTX on the network structure and synchrony of SCN neurons. However, they typically examine data characteristics at a single scale, overlooking variations across different scales. Research has demonstrated that biological neural networks operate at multiple levels of granularity, from individual neurons to local neural circuits and extending to extensive networks comprising thousands of cells.[18] The SCN network is no exception to this principle, as it is a complex structure that operates across multiple temporal and spatial scales. For example, the circadian signals generated by feedback loops of clock gene transcription and translation occur on the scale of a day, while neuronal firing generates signals on the scale of seconds. Such a single scale analysis fails to capture the full dynamic behavior of SCN neuron complexity and synchrony. To gain a comprehensive understanding of the mechanisms underlying SCN neuron functionality, it is crucial to consider their behavior across multiple scales, thereby fully capturing their complex functions and interaction patterns. Additionally, many papers only mention or, at most, qualitatively study the complexity of SCN neurons and networks.[19–22] To our knowledge, no one has quantitatively measured this complexity thus far.

In this study, we introduce the multiscale structural complexity (namely, MSC) method to examine changes in neuronal activity and complexity at both macro and micro levels (*i.e.*, different degrees of coarse-graining).[23] This method is developed based on the approach proposed by Bagrov *et al.*, designed to describe the complexity of image data across multiple spatial scales.[24,25] The resulting structural complexity, as a new measure of complexity, not only considers the different hierarchical organization of SCN system but also focuses on the interaction between local and global features. Hence, unlike traditional complexity measures (such as entropy, fractal dimension, synchrony, etc.), structural complexity can reveal the hidden hierarchical and evolutionary characteristics within SCN system through cross-scale analysis, making it a more promising tool for the study of complex systems. By analyzing structural complexity and local complexity at various scales, we aim to comprehensively understand how TTX affects SCN neurons. This method enables us to capture critical scales of changes in neuronal interactions that traditional methods may overlook. To validate our experimental findings, we employed the Goodwin model to simulate neuronal activity under different coupling strengths, corresponding to various stages of TTX treatment. The consistency between the simulated data and the experimental results underscores the reliability of our observations and highlights the effectiveness of the Goodwin model in capturing the impact of TTX on neuronal complexity.

By integrating experimental data with theoretical models, this study not only corroborates previous research but also uncovers new insights into the effects of TTX on neuronal structural and local complexities. These findings offer valuable contributions to the field of neuroscience, providing a solid foundation for future research aimed at unraveling the intricate mechanisms governing circadian rhythms. This paper is organized as follows. In Section 2, we present (i) the empirical and model data used in this study, and (ii) the description of the MSC method. Section 3 shows the results, including (i) findings derived from the empirical data and (ii) results obtained from the model data. Finally, Section 4 summarizes and discusses the research findings.

2. Data and methods

2.1. Data

2.1.1. Experimental data

The dataset used in this study can be freely downloaded from https://github.com/JohnAbel/scn-resynchronization-data-2016. SCN neuronal tissues were extracted from the brains of five mice and cultured in five separate ex vivo slices. The number of neuronal cells in slices SCN1 through SCN5 were 383, 264, 304, 281, and 228, respectively.

PERIOD2::Luciferase (PER2::LUC) bioluminescence was used to stain the SCN neurons. Gene expression levels were monitored by recording bioluminescence intensity every hour throughout the experiment. A few days after extraction, TTX was added to the neuronal tissues. TTX inhibits neurotransmitter secretion, reducing coupling strength between neurons while preserving physical connections. After six days of TTX treatment, TTX was washed out, allowing neurotransmitter secretion to gradually return to normal levels, thereby restoring neuronal coupling. The number of data points collected for each neuron in each slice (i.e., the length of the bioluminescence recordings) were: 426 for SCN1, 493 for SCN2, 468 for SCN3, 518 for SCN4, and 447 for SCN5. The bioluminescence recordings were divided into three stages: pre-TTX (before TTX application), during-TTX (during TTX application) and post-TTX (after TTX removal). The time points for TTX application and removal for slices SCN1 through SCN5 were as follows: $\text{TTX_time} = [90, 109, 82, 107, 113]$ and $\text{Wash_time} = [234, 252, 224, 240, 242]$, respectively. For more details of the experiment, please see Ref. [16].

2.1.2. Model data

The Goodwin model is based on the negative feedback loop self-oscillation mechanism and is often used to qualitatively describe the model of the circadian rhythm. In this model, the mRNA of the circadian clock gene produces a corresponding circadian clock protein, which promotes the transcription of the inhibitor, and the inhibitor is in turn inhibition of transcription of the clock gene, thus forming a negative

feedback loop.[26–32] The topology of the SCN is still unclear. Simply, this paper considers it as a globally coupled network. The coupling between neurons is through neurotransmitters (mainly VIP, AVP, and GABA), and the Goodwin model after coupling is as follows:

$$\begin{cases} \dot{X}_i = \eta_i\left(\alpha_1 \dfrac{{k_1}^n}{{k_1}^n + {Z_i}^n} - \alpha_2 \dfrac{X_i}{k_2 + X_i}\right) + \alpha_c \dfrac{GF_i}{k_c + GF_i}, \\ \dot{Y}_i = \eta_i\left(k_3 X_i - \alpha_4 \dfrac{Y_i}{k_4 + Y_i}\right), \\ \dot{Z}_i = \eta_i\left(k_5 Y_i - \alpha_6 \dfrac{Z_i}{k_6 + Z_i}\right), \qquad i = 1,2,3,\ldots,N, \\ \dot{V}_i = \eta_i\left(k_7 X_i - \alpha_8 \dfrac{V_i}{k_8 + V_i}\right), \\ F_i = \dfrac{1}{N}\Sigma_{i=1}^{N} V_i, \end{cases} \tag{1}$$

where N represents the number of neurons in the SCN, and the subscript i represents the i-th neuron. It can be seen that in this model a neuron oscillator consists of four variables X, Y, Z, and V, where X, Y, Z are three components of the above negative feedback loop, representing the mRNA of the circadian clock gene, the corresponding circadian clock protein and the inhibitor, respectively. The variable V represents a neurotransmitter capable of completing coupling between neurons, and the average field F is the concentration of neurotransmitters. In addition, n is the Hill coefficient and G is the coupling strength. η_i obeys a normal distribution with a mean of 1, and this parameter enables the natural period of each neuron to follow a normal distribution between $22h$ and $28h$.[33] The α_1, k_1, α_2, k_2, k_3, α_4, k_4, k_5, α_6, k_6, k_7, α_8, k_8, α_c, and k_c are parameters, and the values of each parameter are set as in Ref. [27]: $\alpha_1 = 0.7$ nM/h, $k_1 = 1$ nM, $n = 4$, $\alpha_2 = 0.35$ nM/h, $k_2 = 1$ nM, $k_3 = 0.7/h$, $\alpha_4 = 0.35$ nM/h, $k_4 = 1$ nM, $k_5 = 0.7/h$, $\alpha_6 = 0.35$ nM/h, $k_6 = 1$ nM, $k_7 = 0.35/h$, $\alpha_8 = 1$ nM/h, $k_8 = 1$ nM, $\alpha_c = 0.4$ nM/h, and $k_c = 1$ nM.

The numerical simulation method used in this paper is a fourth-order Runge–Kutta method with a step size of 0.01. The initial value of each variable is a random number between 0 and 1. In order to eliminate the impact of the transient, we will discard the first 1 million steps (i.e., $10000h$) and retain the next 1.5×10^5 steps (i.e., $1500h$) for subsequent calculations. And the number of neurons in the simulation takes $N = 300$.

2.2. Method

The multi-scale structural complexity method (i.e., MSC) is a technique developed based on the approach of measuring image complexity, designed to characterize system complexity using only a scalar time series. This method first converts the scalar time series into a matrix, then analyzes the matrix at different scales to calculate the local complexity and total complexity (also known as structural complexity) of the system. By following these steps, a more comprehensive understanding of the system's multi-scale characteristics can be achieved. The specific steps of this method are as follows.

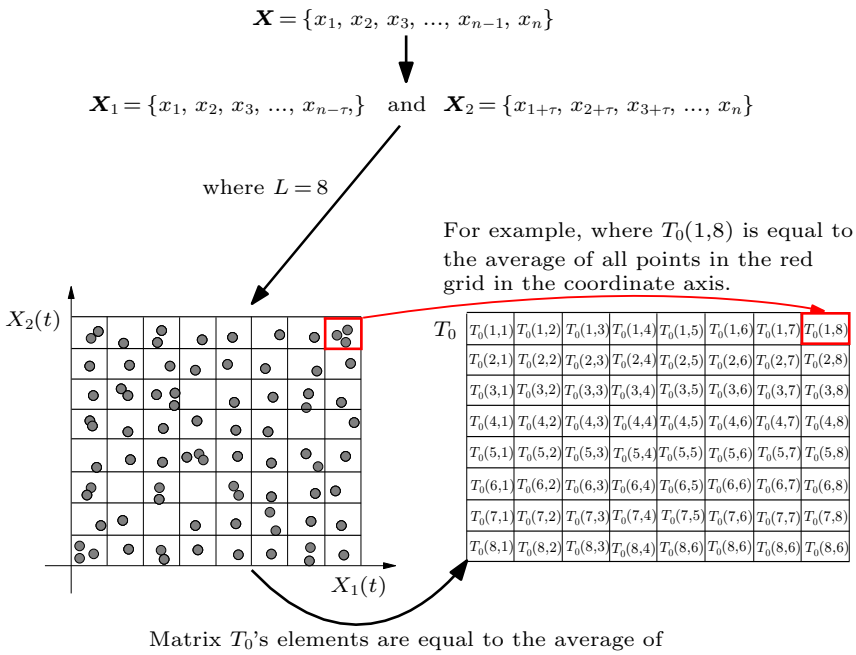


Fig. 1. The process of transforming a scalar time series into a matrix.

Step 1 Converting a scalar time series X into a matrix T_0. First, consider a time series $X = X(1), X(2), \ldots, X(S)$ with a delay time τ. We generate the truncated time series $X_1 = X(1), X(2), \ldots, X(S-\tau)$ and the delayed time series $X_2 = X(1+\tau), X(2+\tau), \ldots, X(S)$, where S is the length of the series. Unless specified otherwise, τ is set to 1. Next, X_1 and

X_2 values are mapped onto the horizontal and vertical axes of a coordinate system, respectively, with the axes spanning the minimum to maximum values of the time series. Each axis is divided into L equal segments, creating a grid of L^2 squares. The mean value of all points within the $(i,j)_{\text{th}}$ square is then calculated and assigned to element $T_0(i,j)$ of matrix T_0. Refer to Fig. 1 for an illustration.

Step 2 Calculating *MSC* for matrix T_0. Initially, the matrix for each scale is calculated. Matrix T_0 is tiled by modules of size $\xi \times \xi$, with ξ set to 2 in this study. Matrix T_1 is generated by averaging the elements within each module of T_0, resulting in T_1 having dimensions $L \times L$ but containing at most $(L/\xi)^2$ distinct values. This process is repeated by covering T_1 with $\xi^2 \times \xi^2$ modules to produce matrix T_2, and so on, generating matrices $T_3, T_4, \ldots, T_n$, where $\xi^n \times \xi^n = L \times L$. Each matrix i is always $L \times L$ in size and represents scale k using at most $(L/(\xi^k))^2$ distinct values. The recursive formula for matrix T_k, representing scale k ($1 \le k \le \log_\xi L$), is as follows:

$$T_k(i,j) = \frac{1}{\xi^k \times \xi^k} \sum_{m=1}^{\xi^k} \sum_{l=1}^{\xi^k} T_{k-1} \times \left(\left\lfloor \frac{i-1}{\xi^k} \right\rfloor \cdot \xi^k + m, \left\lfloor \frac{j-1}{\xi^k} \right\rfloor \cdot \xi^k + l \right), \quad (2)$$

where k represents the scale number and the operator "$\lfloor \cdot \rfloor$" denotes rounding down. Figure 2 illustrates this process.

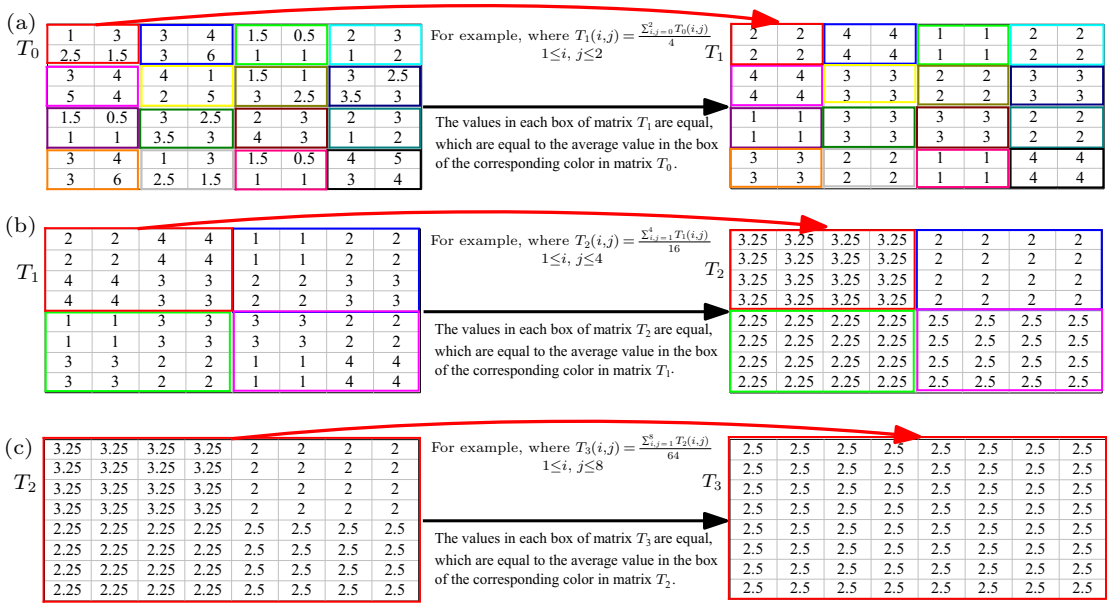


Fig. 2. An illustration of Step 2 for $n = 3$ and $L = 8$. Each $L \times L$ matrix T_i, representing time scale number i, is obtained by tiling the matrix T_i with L/ξ^k modules of size $\xi^k \times \xi^k$ (each represented by a colored box), and averaging values within each module. (a) Obtaining matrix T_1 from matrix T_0 using modules of size $\xi \times \xi$. (b) Obtaining matrix T_2 from matrix T_1 with modules of size $\xi^2 \times \xi^2$. (c) Obtaining matrix T_3 from matrix T_2 using modules of size $\xi^3 \times \xi^3$.

Next, the local complexity for each scale is calculated by assessing how the structure changes with scale. The local complexity C_k at scale k is calculated as the difference between matrices T_{k-1} and T_k, which represent the system at scales $k-1$ and k, respectively. Specifically, the local complexity C_k at scale k is given by

$$C_k = \left| \sum_{i=1}^{L} \sum_{j=1}^{L} O_k(i,j) \right|, \quad (3)$$

where

$$O_k = -\frac{1}{2}(T_k - T_{k-1}) \cdot (T_k - T_{k-1}) = T_k \cdot T_{k-1} - \frac{1}{2}(T_k \cdot T_k - T_{k-1} \cdot T_{k-1}). \quad (4)$$

In these equations, the multiplication "$\cdot$" is element-wise, not matrix multiplication. Finally, the total complexity (that is, structural complexity) is calculated as the sum of the local complexities across all scales:

$$C = \sum_{k=1}^{\log_\xi L} C_k. \quad (5)$$

To clarify, the term "structure" in "structural complexity" refers to the organization and arrangement of a system or signal across different scales, with a particular emphasis on how these elements interact at multiple levels to form an overall complex pattern. It reflects that complexity is not solely determined by local randomness or irregularity, but rather driven by the system's hierarchy, organizational structure, and the relationships between different scales.

3. Results

3.1. Experimental data

Figure 3 shows that (i) the pre-TTX stage, the synchrony among neuronal oscillators was strong, and the oscillators had

relatively large amplitudes; (ii) the during TTX stage, we observe weak circadian rhythms of individual neurons as well as poor synchronization between neurons; (iii) the post-TTX stage was washed out, gradually restoring synchrony among neuronal oscillators. However, compared to the pre-TTX stage, the amplitude and synchrony had not fully returned to their original levels.

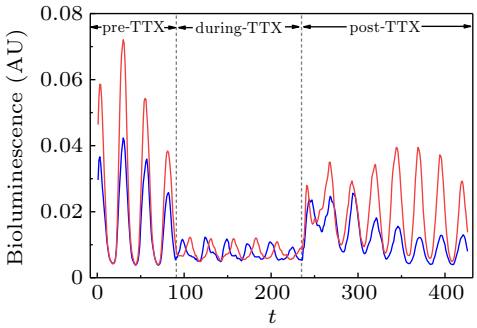


Fig. 3. The time series plot of 2 randomly selected neurons. The recordings are bioluminescence values of PERIOD2::Luciferase (PER2::LUC) from 2 randomly selected neurons in SCN1, showing their time evolution during 3 different stages. The stages pre-TTX, during-TTX, and post-TTX represent the stages before the application of tetrodotoxin, during the application of tetrodotoxin, and after the washout of tetrodotoxin, respectively.

This experimental curve illustrates the process of neuronal oscillators transitioning from synchrony to desynchrony and back to resynchrony throughout the experiment. These results demonstrate that TTX effectively inhibited neuronal coupling, leading to desynchronization, and that removal of TTX allowed for partial resynchronization. This provides a basis for analyzing the complexity of different experimental phases.

Figure 4 shows the comparison of structural complexity C in neurons in slice 1 (i.e., SCN1) during the pre-TTX, during-TTX, and post-TTX stages. The solid symbols represent the average C of 308 neurons in SCN1, and the error bars of the solid symbols indicate the standard error. The stages pre-TTX, during-TTX, and post-TTX correspond to the stages before the application of tetrodotoxin, during the application of tetrodotoxin, and after the washout of tetrodotoxin, respectively. The results show that C is lowest during the during-TTX stage, indicating a significant reduction in the activity and structural complexity of neurons under the influence of TTX. The structural complexity in the post-TTX stage partially recovers but remains lower than in the pre-TTX stage.

The underlying reason for this phenomenon could be that TTX not only inhibits neuronal activity but also alters the coupling strength between neurons. During the during-TTX stage, sodium ion channels are blocked, preventing neurons from generating action potentials normally, thereby reducing the overall activity level of neurons. Simultaneously, the synchronization and coupling strength between neurons decrease, further leading to a reduction in structural complexity. Although neuronal activity partially recovers in the post-TTX stage as TTX is washed out, the complexity does not fully return to the pre-TTX level due to significant changes in neuronal activity and coupling patterns during the during-TTX stage. This comparison allows us to observe the changes in structural complexity due to the application and subsequent removal of tetrodotoxin.

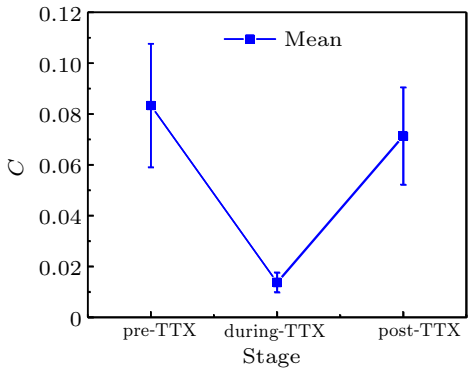


Fig. 4. Comparison of the values of structural complexity C at different stages. The solid symbols represent the average C of 308 neurons in SCN1, and the error bars of the solid symbols indicate the standard error. The stages pre-TTX, during-TTX, and post-TTX correspond to the stages before the application of tetrodotoxin, during the application of tetrodotoxin, and after the washout of tetrodotoxin, respectively. This comparison allows us to observe the changes in structural complexity due to the application and subsequent removal of tetrodotoxin.

In neuroscience, activities at different scales may be interrelated. Multiscale complexity analysis allows for the integration of information across scales, revealing the overall dynamic properties of the system. Figure 5 presents a comparison of local complexity C_k during the pre-TTX, during-TTX, and post-TTX stages. The hollow symbols represent the average C_k of 308 neurons in SCN1, with the error bars indicating the standard error. The variable k represents different coarse-graining scales, with higher values indicating a higher degree of coarse-graining and thus a lower level of precision. The results indicate that (i) with increasing coarse-graining levels (i.e., increasing k), local complexity during the pre-TTX, during-TTX, and post-TTX stages follows a parabolic trend of initially increasing and then decreasing; (ii) during the pre-TTX and during-TTX stages, local complexity peaks at $k = 10$, whereas during the post-TTX stage, local complexity peaks at $k = 9$.

This phenomenon may stem from changes in neuronal interaction patterns and coupling strength induced by TTX treatment. In the pre-TTX stage, neurons are highly synchronized, and their activity patterns become very regular and predictable. At higher coarse-graining levels ($k = 10$), this orderliness is effectively captured, leading to a peak in local complexity. During the TTX stage, neural activity is highly uncoordinated, and the overall activity becomes very random

and disordered. At higher coarse-graining levels ($k = 10$), this randomness and disorder are also captured, again leading to a peak in local complexity. In the post-TTX stage, synchrony among neurons is at an intermediate level, where neural network activity is neither fully ordered nor completely disordered, but somewhere in between. This intermediate level of synchrony is better captured at lower coarse-graining levels ($k = 9$), resulting in a peak in local complexity at these levels. In summary, TTX treatment significantly affects local interaction patterns among neurons, leading to changes in local complexity. These key scales may correspond to important features or mechanisms of the system, and identifying these key scales aids in a deeper understanding of the system's dynamic behavior.

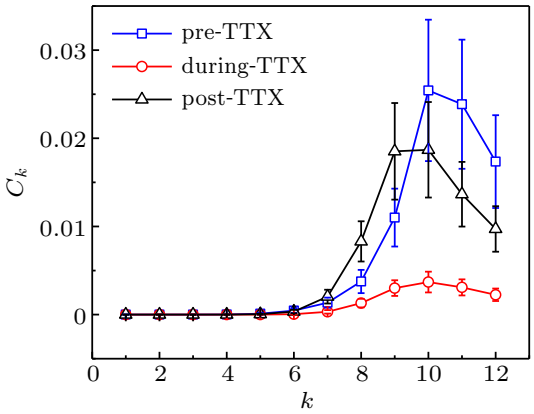


Fig. 5. Comparisons of the values of local complexity C_k at different stages. The hollow symbols represent the average C_k of 308 neurons in SCN1, with the error bars of the hollow symbols indicating the standard error. The variable k represents different coarse-graining scales. The stages before TTX, during TTX, and after TTX correspond to the periods before the application of tetrodotoxin, during the application of tetrodotoxin, and after the removal of tetrodotoxin, respectively. This comparison allows us to observe how local complexity changes across different scales and experimental conditions.

To confirm that the results observed in Figs. 4 and 5 are not coincidental, we extended our analysis to slices 2 through 4 (i.e., SCN2 to SCN4), calculating the structural complexity C and local complexity C_k of neurons in these additional slices.

Figures 6 and 7 present the results of these analyses. The results demonstrate that (i) the structural complexity of neurons in these slices aligns with the slices 1, with the order being $C_{\text{pre-TTX}} > C_{\text{post-TTX}} > C_{\text{during-TTX}}$; (ii) local complexity peaks at a higher coarse-graining level ($k = 10$) during the pre-TTX and post-TTX stages, while it peaks at a lower coarse-graining level ($k = 9$) during the during-TTX stage.

These findings confirm that the results depicted in Figs. 4 and 5 are not coincidental but reflect genuine features of neuronal complexity changes across different treatment stages. The consistency observed across multiple slices enhances our confidence in the reliability of the experimental results and the general applicability of our conclusions.

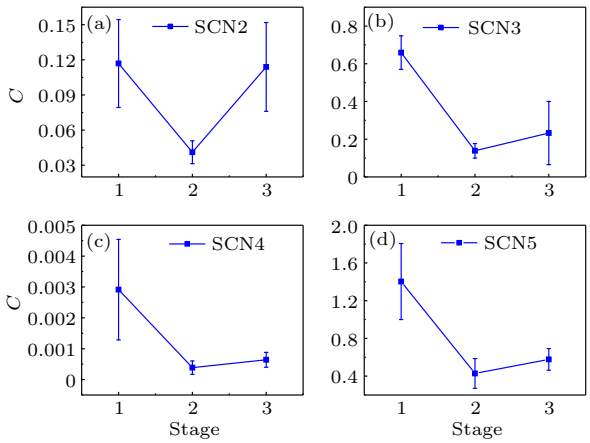


Fig. 6. Comparisons of the values of structural complexity C at different stages. Panels (a)–(d) represent the results for SCN2–SCN4, respectively. The solid symbols represent the average C of all neurons in the corresponding slice, and the error bars of the solid symbols indicate the standard error. The stages pre-TTX, during-TTX, and post-TTX correspond to the stages before the application of tetrodotoxin, during the application of tetrodotoxin, and after the washout of tetrodotoxin, respectively. This comparison highlights the structural complexity changes across different slices and experimental conditions, providing a comprehensive view of how tetrodotoxin affects neuronal network complexity.

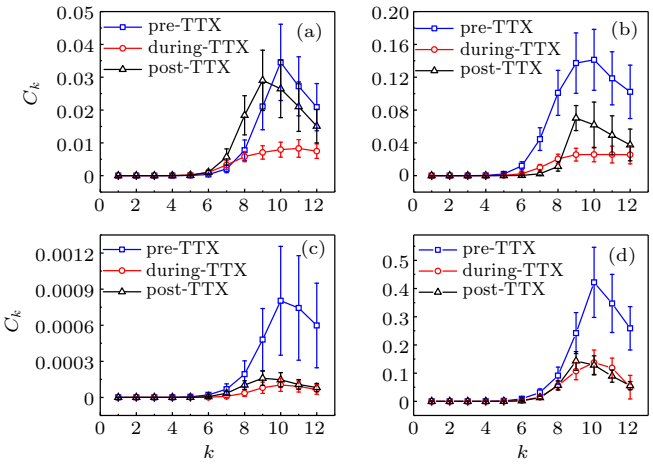


Fig. 7. Comparisons of the values of local complexity C_k at different stages. Panels (a)–(d) represent the results for SCN2–SCN4, respectively. The hollow symbols represent the average C_k of all neurons in the corresponding slice, with the error bars of the hollow symbols indicating the standard error. The variable k represents different coarse-graining scales. The stages before TTX, during TTX, and after TTX correspond to the periods before the application of tetrodotoxin, during the application of tetrodotoxin, and after the removal of tetrodotoxin, respectively. This comparison elucidates how local complexity changes across various slices and conditions, offering a detailed understanding of the impact of tetrodotoxin on the structural complexity at multiple scales. The data provides valuable insights into the dynamic behavior of neuronal networks under different experimental conditions, enhancing our comprehension of their multi-scale properties.

3.2. Model simulations

To validate the experimental data, we employed the Goodwin model to simulate neuronal activity under different coupling strengths. In the simulation, the three stages-pre-TTX, during-TTX, and post-TTX-were modeled by altering the coupling strength G between the oscillators. Specifically, the coupling strengths for the pre-TTX, during-TTX, and post-TTX stages were set to $G = 1$, $G = 0$, and $G = 0.8$, respectively. Hence, the only difference between the models at dif-

ferent stages was the coupling strength. Figure 8 presents the simulated data generated using the Goodwin model, demonstrating that the simulation results are consistent with those in Fig. 3. During the simulation, neuronal oscillators exhibited synchronization and pronounced circadian rhythms during the pre-TTX and post-TTX stages, whereas they lost synchronization and exhibited reduced amplitude during-TTX stage. Thus, these results indicate that the model accurately describes the experimental data.

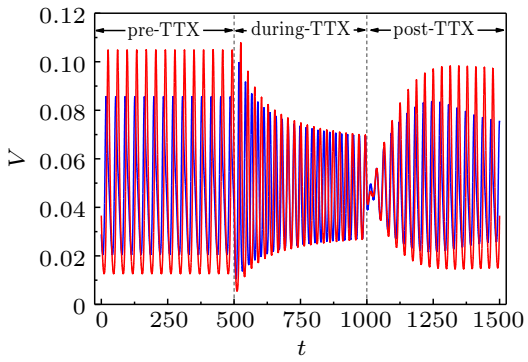


Fig. 8. Temporal evolutions of 2 randomly selected neurons from the Goodwin model simulation. This figure corresponds to Fig. 1. The coupling strengths for the pre-TTX, during-TTX, and post-TTX stages are $G = 1$, $G = 0$, and $G = 0.8$, respectively. These stages correspond to the stages before the application of tetrodotoxin, during the application of tetrodotoxin, and after the washout of tetrodotoxin, as shown in Fig. 3. This allows us to compare the modeled neural activity with the observed data and to understand how changes in coupling strength influence the dynamics of the neuron oscillations.

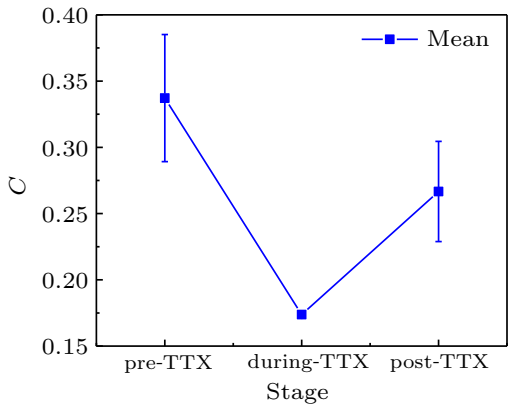


Fig. 9. Numerical results from the Goodwin model. Comparisons of the values of structural complexity C at different stages, as shown in Fig. 2. The solid symbols represent the average structural complexity C of 300 neurons, and the error bars of the solid symbols indicate the standard error. The coupling strengths for the pre-TTX, during-TTX, and post-TTX stages are $G = 1$, $G = 0$, and $G = 0.8$, respectively. These stages correspond to the periods before the application of tetrodotoxin, during the application of tetrodotoxin, and after the washout of tetrodotoxin, as shown in Fig. 4. This comparison highlights how the coupling strength influences the structural complexity of the neuronal network during different experimental conditions.

Subsequently, we calculated the structural complexity (Fig. 9) and local complexity (Fig. 10) of the simulated data. The result in Fig. 9 shows that the structural complexity of the simulated data aligns with the experimental data, with the order being $C_{\text{pre-TTX}} > C_{\text{post-TTX}} > C_{\text{during-TTX}}$. Figure 10 demonstrates that the trend of local complexity at different k values also matches the experimental results, showing a parabolic shape. Notably, there is a slight difference from the experimental data: the peaks of local complexity for the pre-TTX and during-TTX stages in the simulation occur at $k = 4$, while the peak for the post-TTX stage occurs at $k = 5$. This difference suggests a significant change in neuronal interaction patterns during the post-TTX stage.

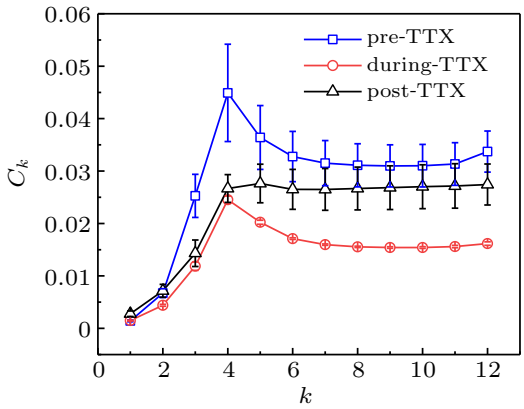


Fig. 10. Numerical results from the Goodwin model. Comparisons of the values of local complexity C_k at different stages, as shown in Fig. 3. The hollow symbols represent the average C_k of 300 neurons, with the error bars of the hollow symbols indicating the standard error. The variable k represents different coarse-graining scales. The coupling strengths for the pre-TTX, during-TTX, and post-TTX stages are $G = 1$, $G = 0$, and $G = 0.8$, respectively. These stages correspond to the periods before the application of tetrodotoxin, during the application of tetrodotoxin, and after the washout of tetrodotoxin, as shown in Fig. 5. This comparison provides insight into how local complexity changes across different scales and experimental conditions, allowing for a deeper understanding of the system's behavior in response to the presence of tetrodotoxin.

The slight discrepancy between the model simulation results and the experimental data regarding the coarse-graining levels at which local complexity peaks can be explained from multiple perspectives, including experimental conditions, model assumptions, and the inherent complexity of neural networks. However, overall, the simulation results of the Goodwin model further validate the reliability of the experimental data. In summary, TTX treatment significantly impacts the local interaction patterns among neurons, leading to changes in local complexity.

4. Discussion and conclusion

The suprachiasmatic nucleus (SCN), as the core region of the mammalian biological clock, regulates circadian rhythms and various physiological functions. In recent years, significant progress has been made in the study of the complexity and synchrony of SCN neurons, especially regarding their states before, during, and after the application of tetrodotoxin (TTX).[16,17] These studies provide valuable theoretical basis for understanding the effects of TTX on the complexity and

synchrony of SCN neurons. However, most studies have focused only on changes in neuronal electrical activity, with less discussion on structural complexity and local complexity. Additionally, previous research mainly focused on experimental observations, lacking validation through theoretical models.

This study, by introducing multiscale complexity analysis, not only examines changes in neuronal activity on a macro level but also reveals the patterns of local complexity changes on a micro level. It demonstrates a comprehensive focus on the multilevel, multiscale organization and dynamic interactions of the SCN, extending traditional complexity measures and providing a better understanding of the SCN system's hierarchical structure and cross-scale relationships. Firstly, the experimental data show that in the pre-TTX phase, the synchrony among neuronal oscillators is strong, with large amplitudes; in the during-TTX phase, the amplitude and coupling strength between oscillators are obviously weakened, which leads to the decrease of synchronization; in the post-TTX phase, TTX is washed out, gradually restoring synchrony among neuronal oscillators, although the amplitude and synchrony do not fully return to pre-TTX levels.

By comparing the structural complexity C, the result shows that during the TTX phase, C is the lowest, indicating a significant reduction in neuronal activity and structural complexity under the influence of TTX. In the post-TTX phase, C partially recovers but remains lower than in the pre-TTX phase. This suggests that TTX not only inhibits neuronal activity but also alters the coupling strength between neurons.

In addition, the local complexity analysis reveals that local complexity C_k follows a parabolic trend of initially increasing and then decreasing with increasing coarse-graining levels, and this trend varies at different stages. Specifically, the peaks of local complexity for pre-TTX and during-TTX stages in the simulation occur at the same k (i.e., $k = 10$), while the peak for the post-TTX stage occurs at a different k (i.e., $k = 9$). This indicates that both high and low synchrony among neurons lead to a peak in local complexity at higher coarse-graining levels, while medium synchrony results in a peak in local complexity at lower coarse-graining levels. This phenomenon can be explained by the coordination and randomness of neural networks: highly synchronized neurons exhibit very regular and predictable activity patterns, captured effectively at higher coarse-graining levels, leading to a peak in complexity. Conversely, highly uncoordinated neural activity becomes very random and disordered, also peaking at higher coarse-graining levels. Intermediate synchrony among neurons results in neural network activity that is neither fully ordered nor completely disordered, better captured at lower coarse-graining levels, leading to a peak in complexity at these levels. Identifying these key scales is crucial for gaining a deeper understanding of the system's dynamic behavior, as they correspond to important features or mechanisms of the system.

To validate the reliability of the experimental data, we employed the Goodwin model to simulate neuronal activity under different coupling strengths. The simulation results show that the trend of complexity changes in the simulated data is consistent with the experimental data, further validating the reliability of the experimental results. This indicates that the Goodwin model can effectively describe the effects of TTX on neuronal complexity.

In summary, by integrating experimental data and model simulations, this study not only validates the results of previous research but also further reveals the effects of TTX on neuronal structural complexity and local complexity. These findings provide new perspectives for neuroscience research and lay the foundation for future studies.

Despite the significant findings of this study, several limitations remain. For instance, while we have discovered that the application of TTX may affect the key scales at which local complexity peaks, the specific mechanisms underlying this effect are not yet clear. Furthermore, these key scales may correspond to important features or mechanisms of the system. Identifying and understanding these key scales will help to reveal the dynamic behavior of the system more deeply. Therefore, future research should aim to investigate the specific mechanisms by which TTX affects these key scales and further elucidate their relationship to the overall function of the system through various approaches. This will provide a more comprehensive understanding and offer new research perspectives in the field of neuroscience.

Acknowledgements

Project supported by the National Natural Science Foundation of China (Grant Nos. 12275179, 11875042, and 12150410309) and the Natural Science Foundation of Shanghai (Grant No. 21ZR1443900).

References

[1] Pittendrigh C S and Daan S 1976 *Journal Of Comparative Physiology A-Neuroethology Sensory Neural and Behavioral Physiology* **106** 223
[2] Pittendrigh C S 1993 *Annual Review of Physiology* **55** 16
[3] Refinetti R 2006 *Circadian Physiology* 2nd edn. (Boca Raton, Florida: CRC Press)
[4] Welsh D K, Takahashi J S and Kay S A 2010 *Annual Review of Physiology* **72** 551
[5] Abraham U, Granada A E, Westermark P O, *et al*. 2010 *Molecular Systems Biology* **6** 438

[6] Campuzano A, Vilaplana J, Cambras T, *et al*. 1998 *Physiology and Behavior* **63** 171
[7] Hastings M H, Maywood E S and Brancaccio M 2018 *Nature Reviews Neuroscience* **19** 453
[8] Michel S and Meijer J H 2020 *European Journal of Neuroscience* **51** 482
[9] Mohawk J A and Takahashi J S 2011 *Trends in Neurosciences* **34** 349
[10] Nakamura W, Yamazaki S, Takasu N N, *et al*. 2005 *The Journal of Neurosciences: the Official Journal of the Society for Neuroscience* **25** 5481
[11] Liu C, Weaver D R, Strogatz S H, *et al*. 1997 *Cell* **91** 855
[12] Ohta H, Yamazaki S and McMahon D G 2005 *Nature Reviews. Neuroscience* **8** 267
[13] Yamaguchi S, Isejima H, Matsuo T, *et al*. 2003 *Science* **302** 1408
[14] Abel J H 2018 *A Computational Approach to Analysis and Control of the Mammalian Circadian Oscillator*
[15] Schmal C, Herzog E D and Herzel H 2018 *Journal of Biological Rhythms* **33** 84
[16] Abel J H, Meeker K, Granados-Fuentes D, *et al*. 2016 *Proc. Natl. Acad. Sci. USA* **113** 4512
[17] Gu C, Gu X, Wang P, *et al*. 2019 *Journal of Biological Rhythms* **34** 515
[18] Yoshikawa T, Pauls S, Foley N, *et al*. 2021 *eNeuro* **8** ENEURO.0078-21.2021
[19] Comas M, De Pietri Tonelli D, Berdondini L, *et al*. 2024 *Trends in Neurosciences* **47** 36
[20] Gillette M U, DeMarco S J, Ding J M, *et al*. 1993 *Journal of Biological Rhythms* **8** Suppl S53–58
[21] Mitchell J W, Atkins N Jr, Sweedler J V, *et al*. 2011 *Frontiers in Neuroendocrinology* **32** 377
[22] Mesgar S, Eskandari K, Karimian-Sani-Varjovi H, *et al*. 2023 *Neurochemical Research* **48** 3420
[23] Wang P, Gu C G, Yang H J, *et al*. 2023 *Physica A* **609** 128358
[24] Bagrov A A, Iakovlev I A, Iliasov A A, *et al*. 2020 *Proc. Natl. Acad. Sci. USA* **117** 30241
[25] Wang P, Gu C G, Yang H J, *et al*. 2022 *Chaos Soliton. Fract.* **164** 112721
[26] Locke J C, Westermark P O, Kramer A, *et al*. 2008 *BMC Systems Biology* **2** 22
[27] Gonze D, Bernard S, Waltermann C, *et al*. 2005 *Biophysical Journal* **89** 120
[28] Gu C G, Wang J X, Wang J X, *et al*. 2011 *Phys. Rev. E* **83** 046224
[29] Xu J S, Gu C G, Pumir A, *et al*. 2012 *Phys. Rev. E* **86** 041903
[30] Gu C G, Xu J S, Liu Z H, *et al*. 2013 *Phys. Rev. E* **88** 022702
[31] Gu C G, Liang X M, Yang H J, *et al*. 2016 *Scientific Reports* **6** 21412
[32] Hafner M, Koeppl H and Gonze D 2012 *PLoS Computational Biology* **8** e1002419
[33] Honma S, Nakamura W, Shirakawa T, *et al*. 2004 *Neuroscience Letters* **358** 173